Electric and magnetic properties of the stage-2 $FeBr_2$ graphite intercalation compound

2003 J. Phys.: Condens. Matter 15 203

(http://iopscience.iop.org/0953-8984/15/2/320)

INSTITUTE OF PHYSICS PUBLISHING JOURNAL OF PHYSICS: CONDENSED MATTER

J. Phys.: Condens. Matter **15** (2003) 203–215 PII: S0953-8984(03)38121-4

Electric and magnetic properties of the stage-2 $FeBr_2$ graphite intercalation compound

P A Dube, M Barati[1], P K Ummat, G Luke and W R Datars[2]

Department of Physics and Astronomy, McMaster University, Hamilton, ON, L8S 4M1, Canada

E-mail: datars@mcmaster.ca

Received 13 June 2002
Published 20 December 2002
Online at stacks.iop.org/JPhysCM/15/203

Abstract

The stage-2 $FeBr_2$ graphite intercalation compound (GIC) was prepared by reacting $FeBr_2$ powder and highly oriented pyrolytic graphite in a bromine atmosphere at 500 °C for 40 weeks. The dc magnetization, ac susceptibility, specific heat, resistivity and Hall effect were measured. The GIC is paramagnetic at temperatures above 14.5 K. There is short-range ordering at 14.5 K and longer-range magnetic ordering at 8.5 K. There is a spin glass phase below 3.2 K in which the ac susceptibility is frequency dependent. The in-plane and c-axis resistivities result from in-plane and out-of-plane electron–phonon scattering. The Hall coefficient is independent of temperature between 4.2 and 300 K and is explained by the single-carrier model.

1. Introduction

$FeBr_2$ has been studied extensively because it has antiferromagnetic ordering below 14.2 K. In the ordered phase, spins in the ab plane are parallel but are aligned antiparallel with spins in the adjacent planes to form an antiferromagnetic state. It is magnetomorphic with a field-induced phase transition below the Néel temperature from the antiferromagnetic to a paramagnetic phase. There have been recent studies of these phases with neutron diffraction [1], specific heat [2], magnetometry [3] and the Mössbauer effect [4] which have resulted in a detailed understanding of the phase diagram of $FeBr_2$.

The compound $FeBr_2$ has the hexagonal CdI_2 structure with $a = 3.772$ Å and $c = 6.223$ Å. There are Fe^{2+} layers separated by Br^- bilayers along the c axis. Thus $FeBr_2$ is layered with nearly two-dimensional magnetic characteristics.

Despite the large number of studies of the magnetic metal-chloride graphite intercalation compounds (GICs) that have been performed [5], there has been very little accomplished with

[1] Permanent address: Department of Physics, Shiraz University, Shiraz, Iran.
[2] Author to whom any correspondence should be addressed.

0953-8984/03/020203+13$30.00

the corresponding bromides because of the difficulty of preparing samples. Balestri *et al* [6] attempted to intercalate metal bromides into natural graphite flakes and pyrolytic graphite by using the two-zone method and concluded that the bromides do not intercalate as readily as the analogous chlorides. In 1977, Stahl [7] was able to intercalate $FeBr_2$ into powdered graphite with limited success and reported values of 22.8, 13.3 and 9.9 Å for the *c*-axis repeat distances of stages 5, 2 and 1 $FeBr_2$ GIC, respectively. In the summary of metal bromides that had been intercalated up to 1977, Stumpf [8] noted that relatively few metal bromides had been intercalated. However, later Stumpf *et al* [9] synthesized $NiBr_2$ and $CoBr_2$ GICs by an intercalant exchange method. $FeBr_2$ was not intercalated into highly oriented pyrolytic graphite and there have been no reports of the magnetic and electrical transport properties of the $FeBr_2$ graphite compounds.

The purpose of this paper is to report magnetic and electrical transport properties of the stage-2 $FeBr_2$ GIC. The method of sample preparation and the techniques of measurement are given in section 2. The magnetization and the ac and dc susceptibility measurements as a function of temperature for different applied magnetic fields are presented in section 3. The specific heat for temperatures between 3 and 11 K is also presented. Finally, the electrical resistivity and Hall coefficient are shown as a function of temperature and the angular dependence of the magnetoresistance is presented. The nature of the magnetic phases and the transport properties are discussed in section 4 and the conclusions are given in section 5.

2. Experimental method

Highly oriented pyrolytic graphite (HOPG) was cleaved into pieces with a thickness of approximately 0.3 mm. They were washed in acetone, ultrasonically cleaned and dried in a vacuum at an elevated temperature. The $FeBr_2$ powder is hygroscopic and reacts with moisture in the air to form a hydrated compound. Therefore, the handling was done in a dry box filled with argon. Several pieces of HOPG were covered with $FeBr_2$ powder in a reaction tube, which was capped for removal from the dry box and then attached to a specially designed vacuum line, evacuated, back-filled with a bromine atmosphere and sealed. The tube was then placed in a small box furnace at 500 °C for 40 weeks to produce the stage-2 $FeBr_2$ GIC. Attempts to create other stages, in particular the stage-1 compound, were not successful. This emphasizes the difficulty of preparing the metal bromide GICs. The stage-2 $FeBr_2$ was characterized by (001) x-ray diffraction as shown in figure 1. The spectrum reveals a single stage with a *c*-axis period I_c of 13.14 Å.

The dc magnetization experiments were performed with a Quantum Design MPMS magnetometer. It was comprised of a SQUID detector and a superconducting magnet with components for temperature control, gas handling and liquid helium, all of which were computer controlled. The zero-field-cooled (ZFC) measurements were done by cooling the sample in zero field and then applying a magnetic field for the measurements during warming. For the field-cooled (FC) measurements, data were taken during cooling with an applied magnetic field.

The ac susceptibility and specific heat measurements were taken with an Oxford Instruments Mag Lab EXA system. For the susceptibility measurements, an ac current in a primary coil induced ac currents in two secondary coils. The sample was in one coil and the signal from it was subtracted from that of the second coil. Both the real and imaginary parts were detected with a lock-in amplifier.

The heat capacity measurements were obtained by using the relaxation method. The time constant of the exponential decay of the temperature of the sample platform after it was heated by a stepwise change of heat was determined from which the specific heat was derived.

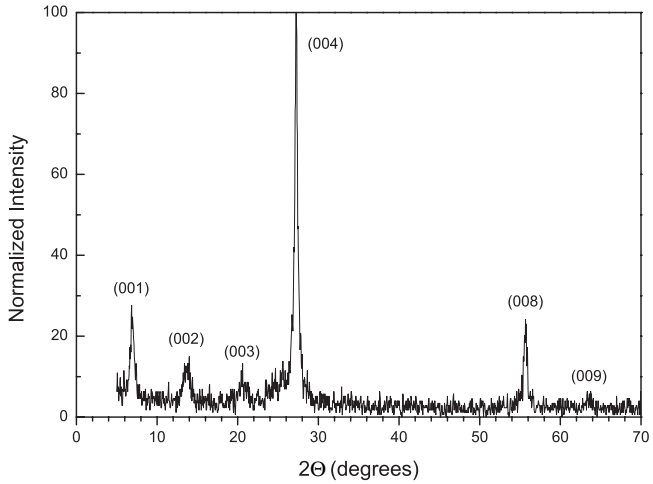

Figure 1. (001) x-ray diffractogram of a stage-2 $FeBr_2$ sample with Cu Kα radiation. The indexed peaks are for the stage-2 compound.

The in-plane resistivity was measured by the standard four-probe technique and by the Montgomery method [10] in which the contacts were made to the corners of a rectangular sample. The electrical contacts were formed with silver paste. The *c*-axis resistivity was measured with the current contacts and the potential contacts on opposite sides of the cleaved surfaces of a sample. The Hall voltage was determined with the magnetic field from an electromagnet parallel to the *c* axis and mutually perpendicular current and potential probes in the (001) plane. Pairs of measurements taken before and after the sample was rotated 180° about the current direction were used to determine the odd component of the voltage with respect to the field direction and to cancel the voltage caused by a small misalignment of the probes.

3. Experimental details

The low temperature dc susceptibility in figure 2 was taken with an applied field of 2 Oe perpendicular to the *c* axis. There are changes in the susceptibility at 14.5 and 8.5 K. There is also a difference between the ZFC and FC data beginning at 14.5 K. Finally, at 3.2 K there is a maximum in the ZFC susceptibility and a change of slope in the FC data. The discontinuity at 4.4 K in the ZFC data taken during warming is a result of the sample magnetization relaxing under the influence of an applied field at a constant temperature over a period of time. To cool the sample below 4.3 K, the sample space is filled with liquid helium and the vapour pressure is reduced by a vacuum pump. In order to raise the temperature above 4.3 K, this helium is boiled off. The boiling process takes approximately 20 min, during which time the field is left on. The magnetic moments relax with a characteristic time to align themselves along the direction of the applied field. This relaxation time, though not explicitly measured, is observed to be of the order of tens of minutes. The result is that the magnetization increases sharply between data points when the temperature is increased through 4.3 K.

The separation between the ZFC and FC data below 14.5 K decreases as the applied field is increased as shown in figure 3. With a field of 100 Oe there is little difference between the ZFC and FC curves above the temperature of the 3.2 K peak and there are no sharp changes at 8.5

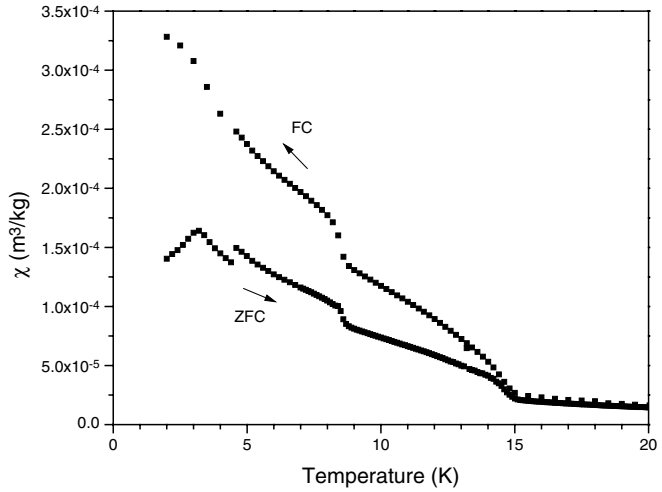

Figure 2. Low temperature dc susceptibility as a function of temperature of the stage-2 $FeBr_2$ GIC showing ZFC and FC data with an applied field of 2 Oe perpendicular to the *c* axis.

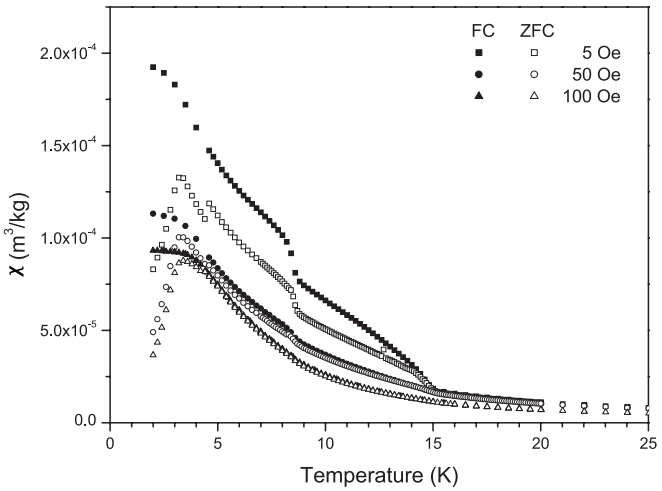

Figure 3. Low temperature dc susceptibility of stage-2 $FeBr_2$ GIC for in-plane applied fields of 5, 50 and 100 Oe.

and 14.5 K. Also the size of the low temperature ZFC peak is smaller and the FC magnetization is saturated below 3.5 K with the higher applied field.

The *c*-axis dc susceptibility is shown in figure 4 for applied fields of 10, 50 and 100 Oe. The magnitude of the susceptibility is smaller than that of the in-plane susceptibility, as shown by the scale. At 100 Oe, the peak at 3.2 K and the steps at 8.5 and 14.5 K are all present, as is the remnant magnetization, shown by the difference between the ZFC and FC data. The ZFC measurements have very little dependence on the applied field.

The ac susceptibility is shown in figure 5. The dispersion χ' has a peak at 4.5 K and shoulders at 8.5 and 14.5 K. The absorption χ'' has peaks at 14.5, 8.5 and 4 K. The frequency dependence of χ' is shown in figure 6. With increasing frequency, the lowest temperature peak

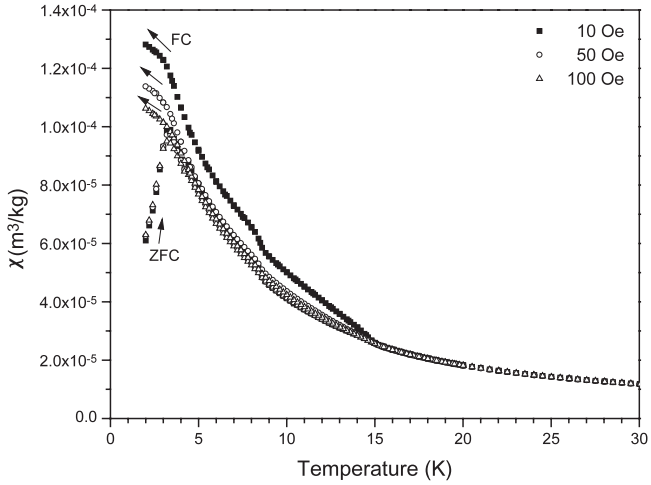

Figure 4. Low temperature dc susceptibility of the stage-2 $FeBr_2$ GIC with magnetic fields of 10, 50 and 100 Oe applied along the c axis. ZFC and FC data are shown.

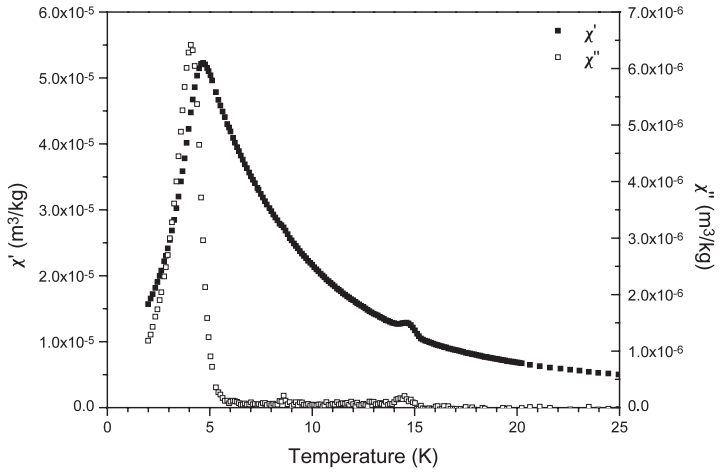

Figure 5. The dispersion χ' and the absorption χ'' of the ac susceptibility of the stage-2 $FeBr_2$ GIC as a function of temperature.

moves to higher temperature and decreases in magnitude. There is no discernible effect of frequency on the changes at 8.5 and 14.5 K.

Specific heat measurements of the stage-2 $FeBr_2$ GIC are shown in figure 7, plotted in the standard form of C/T versus T^2. There is a peak at 8.5 K which matches the temperature of the peak in both the ac and dc susceptibility. There are no features at 3.2 and 14.5 K for which there are features in the susceptibility. With the application of a magnetic field, the peak size decreases and completely disappears at 3 T, as shown in figure 7.

The resistivities ρ_a and ρ_c measured with the current perpendicular and parallel to the c axis, respectively, are presented in figure 8 for the temperature range 4.2–300 K. ρ_a has a value of 8.8×10^{-4} Ω cm at 4.2 K and increases to 13×10^{-4} Ω cm at room temperature, indicating an increase of 48% in this range of temperature.

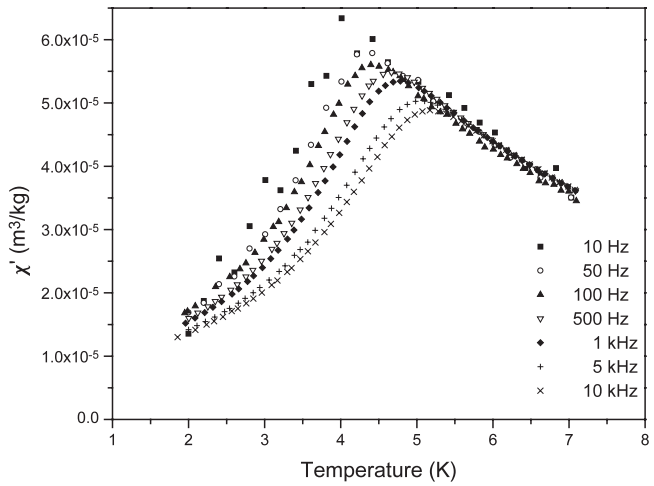

Figure 6. The in-plane ac susceptibility dispersion of the stage-2 $FeBr_2$ GIC as a function of temperature between 2 and 7 K for different applied frequencies.

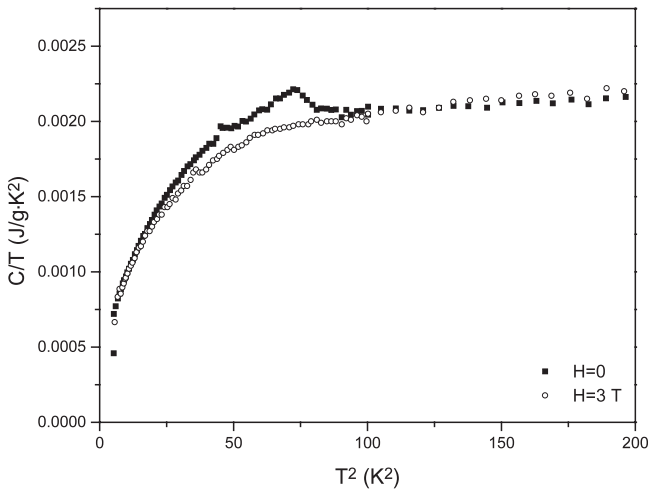

Figure 7. Specific heat of the stage-2 $FeBr_2$ GIC divided by T plotted against T^2 with applied fields of 0 and 3 T.

The angular dependence of the c-axis magnetoresistance for a set of fields between 3 and 9 T is given in figure 9. The field is parallel to the ab plane at $\theta = 0°$ and parallel to the c axis at $\theta = 90°$. The minimum magnetoresistance occurs with the field in the ab plane and the maximum is with the field parallel to the c axis. At all fields the angular dependence has a $\cos^2\theta$ dependence. This indicates that two-dimensional effects are not present.

The temperature dependence of the Hall coefficient R_H measured with a magnetic field of 1 T along the c axis and a current of 100 mA perpendicular to the c axis is presented in figure 10. The Hall coefficient is independent of temperature to within experimental uncertainty and has a value of $(4.5 \pm 0.5) \times 10^{-8}$ m^3 C^{-1}. The data points and their standard deviations in the figure were determined from the average of approximately 20 measurements in a range of 10 K around each point. The experiment was also performed with different currents and magnetic fields. No significant change in the Hall coefficient was observed.

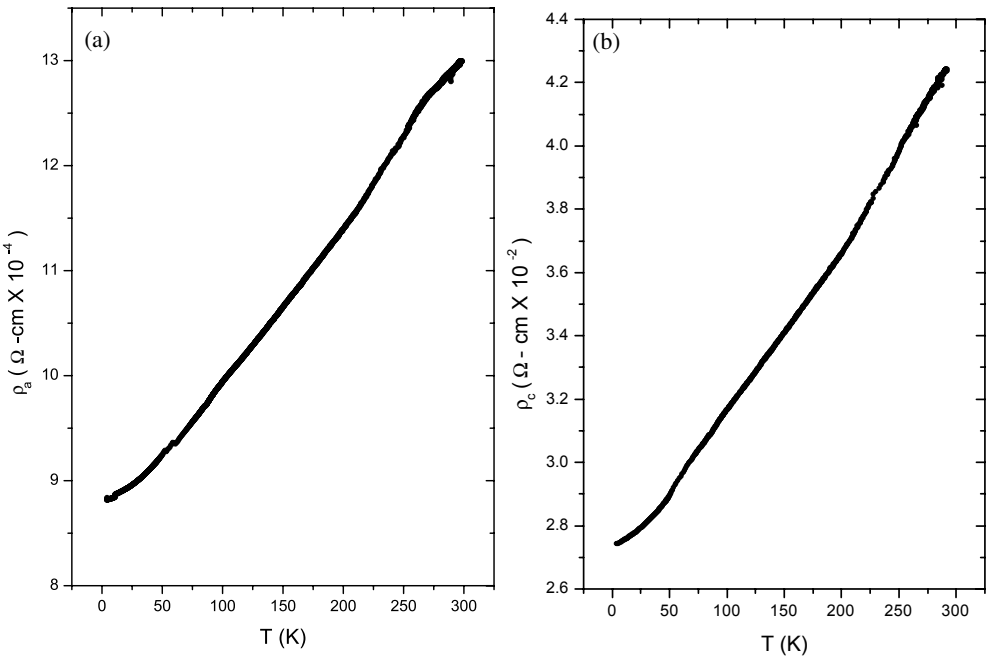

Figure 8. (a) The resistivity ρ_a of the stage-2 $FeBr_2$ GIC as a function of temperature. (b) The resistivity ρ_c as a function of temperature.

4. Discussion

The magnetic susceptibility in the paramagnetic region, plotted in figure 11 in the standard form of $1/\chi$ versus T, is fit to the Curie–Weiss law $\chi = C/(T - \theta_{CW})$, where θ_{CW} is the Curie–Weiss constant. We show that an improvement is seen at low temperatures with the addition of a temperature-independent susceptibility

$$\chi = \chi_o + C/(T - \theta_{CW})$$

where χ_o is the van Vleck susceptibility, improves the fit in figure 11 at temperatures below 100 K. van Vleck paramagnetism has been shown to occur in pristine $FeBr_2$ [11] as well as in other iron halides [12, 13]. This effect has also been observed in other metal-halide GICs [14, 15]. The parameters from the fit, obtained by using a standard nonlinear least squares curve fitting routine, are $C = (1.35 \pm 0.01) \times 10^{-4}$ K m^3 kg^{-1}, $\theta_{CW} = 5.1 \pm 0.7$ K and $\chi_o = (5.7 \pm 0.4) \times 10^{-8}$ m^3 kg^{-1}. From the value of the Curie constant and assuming the effective moment $u_{eff} = 5.6u_B$ of $FeBr_2$, the number of moments is 1.73×10^{19} cm^{-3}. With one moment on each $FeBr_2$ ion, the C:$FeBr_2$ ratio is 12.5. The maximum packing density calculated for this material is 9.4, giving a filling factor of 75%, which is quite good compared with other metal-halide GICs.

The magnetization of a sample in the spin glass phase is highly dependent on its history. The property of history dependence is present in the dc magnetization measurements in figure 2 because the susceptibility has a maximum at the freezing temperature $T_F = 3.2$ K during warming in a magnetic field. The magnetization increases as the temperature increases to T_F as the moments align with the magnetic field. Above T_F the magnetization decreases as random thermal motion decreases the net magnetization. When the sample is cooled in a magnetic field the moments align along the field as the temperature decreases to T_F. The moments are frozen below T_F and the sample maintains a finite magnetization as observed in figure 2.

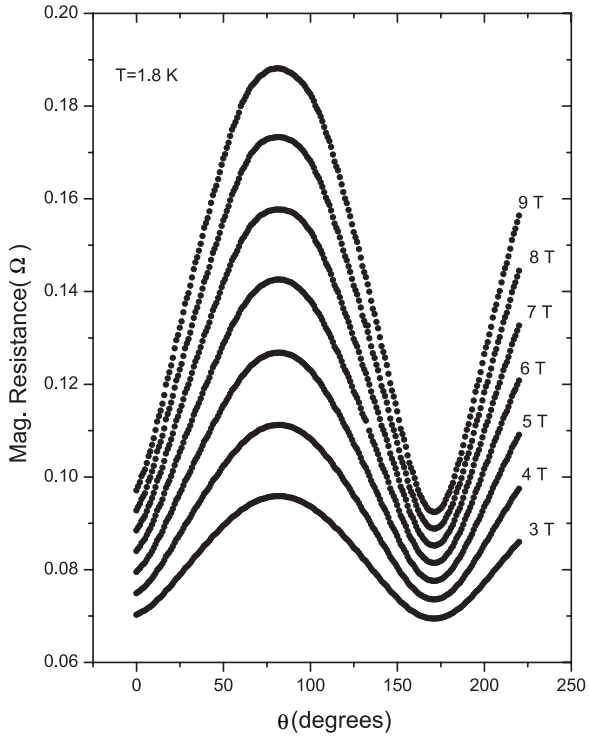

Figure 9. The *c*-axis resistance of the $FeBr_2$ GIC as a function of the direction of the magnetic field with respect to the (001) plane for a set of applied fields.

In the ac susceptibility measurements shown in figure 5, the dispersion χ' increases approximately as $1/T$. χ' decreases near the freezing temperature as the motion of the moments becomes stiffer and drops to zero slightly below T_F. The absorption, χ'', increases as the relaxation time of the system increases and then decreases to zero as the temperature decreases further. The result is that the peak in χ' is at a higher temperature than that of χ'', and corresponds to a maximum in $\mathrm{d}\chi''/\mathrm{d}T$. The maximum slope in the imaginary component indicates the onset of freezing, which corresponds to the point where the susceptibility starts to decrease with decreasing temperature because of increased difficulty in moving the magnetic moments.

The frequency dependence of χ' shown in figure 6 is expected in the spin glass phase. As the frequency increases, the temperature at the peak increases and the magnitude of the peak decreases because of the relaxation time involved in the spin glass. The frequency dependence of the peak temperature can be fitted to an Arrhenius law. A much better fit, except at low frequencies, shown in figure 12 is obtained by using the Vogel–Fulcher law originally used to describe the viscosity of supercooled liquids:

$$f = f_o \exp(E_a/(k_B(T - T_o)))$$

where T_o is a temperature lower than the freezing temperature and E_a is the activation energy for a thermally excited process with $f_o = (9\pm3)\times10^{13}$ Hz, $E_a/k_B = (9.5\pm1)$ K and $T_o = 1$ K. No physical interpretation is made of E_a and f_o because this law is used only empirically to describe the frequency dependence of spin glasses [16]. While T_o is significantly lower than T_f, it is of the same order of magnitude. We do not compare f_o to values seen in canonical

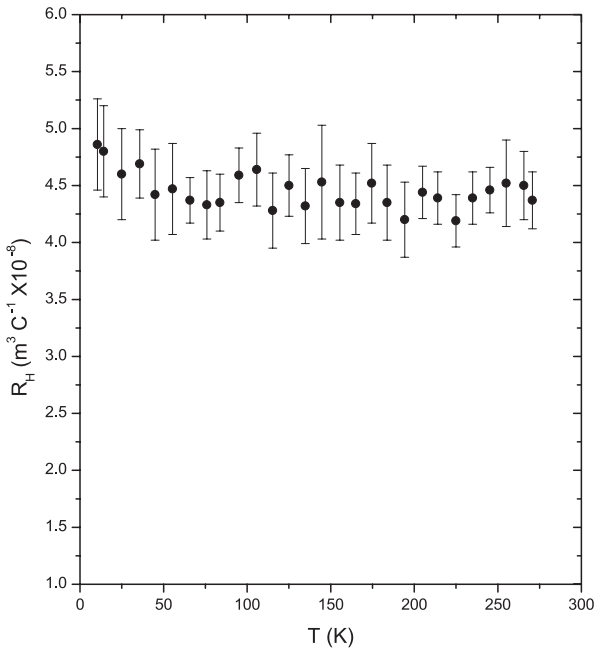

Figure 10. The Hall coefficient of the stage-2 $FeBr_2$ GIC as a function of temperature.

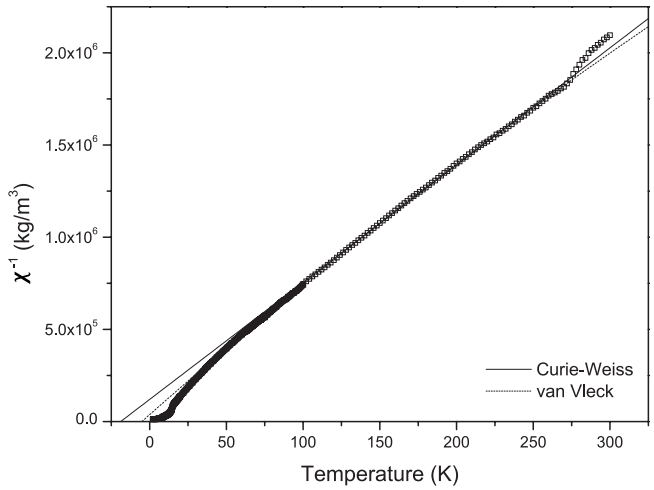

Figure 11. The inverse dc susceptibility versus temperature for the stage-2 $FeBr_2$ GIC. The full line is a standard Curie–Weiss fit and the broken curve is a fit that includes the modification with a temperature-independent van Vleck term, χ_o, as described in the text.

spin glasses since we expect this compound to behave as a cluster glass rather than a canonical spin glass. Mydosh [16] shows that, empirically, the magnitude of $x = \Delta T_f / T_f \ln(\Delta\omega)$ can be used as a measure for distinguishing between spin glasses and superparamagnets. The value of $x = 0.01$–0.06 occurs in canonical spin glasses, $x = 0.6$–0.8 for the insulating spin glasses and $x = 0.28$ for a superparamagnet. The value obtained for our compound, from the frequency dependence shown in figure 6, is $x = 0.12$, closer to the range of insulating

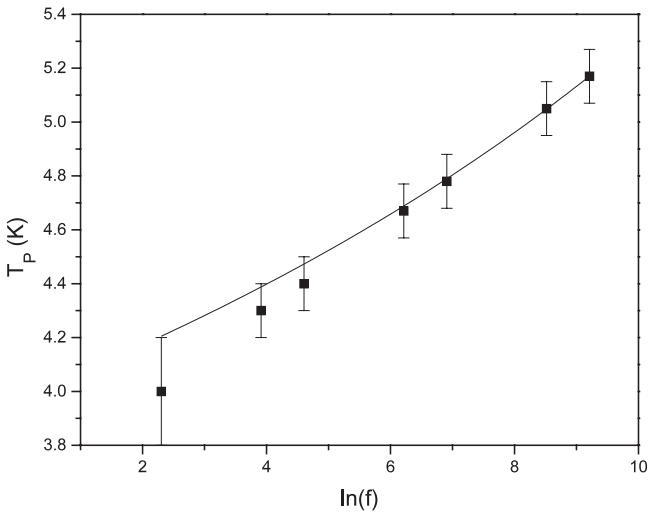

Figure 12. The frequency dependence of the temperature of the peak at the spin glass transition of the stage-2 $FeBr_2$ GIC fit to the Vogel–Fulcher law.

spin glasses than to that of the superparamagnet. This frequency dependence supports the interpretation of the spin glass state because a superparamagnetic phase should have a much larger frequency dependence and there should be no frequency dependence for a transition to an antiferromagnetic state.

The specific heat measurements taken with a field of 3 T are in the high-field region for which there should be no magnetic contributions to the specific heat. The magnetic contributions to the zero-field specific heat can therefore be calculated by subtracting the high-field specific heat from the zero-field specific heat and is given in figure 13. The Gaussian fits to the two peaks are used merely as a convenience for estimating the area under the curve. The broad peak, centred at approximately 7 K, is most likely associated with the glass transition because typically there is not a sharp peak at the freezing temperature but rather a broad peak at a temperature significantly higher than the freezing temperature. The change in entropy associated with the magnetic ordering to the glass state is $(6.8 \pm 0.2) \times 10^{-4}$ J g^{-1} K^{-1}. This represents a change in entropy of only 0.075 ± 0.002 J mol^{-1} K^{-1}. One could expect a value of $S = Nk_B \ln(2J + 1) = 13.4$ J mol^{-1} K^{-1}, where $J = 2$ is the spin number for Fe^{2+}, if the number of spins found in the modified Curie–Weiss fit are ordered during the transition. The large difference is indicative of a high degree of frustration in the low temperature state.

The sharp peak in the magnetic specific heat at 8.5 K is associated with the magnetic ordering that is seen at this temperature in the susceptibility. This may be caused by the long-range ferromagnetic ordering or antiferromagnetic ordering in the sample but the increase in χ_{dc} at this point indicated ferromagnetic ordering. It is unlikely that it is complete three-dimensional ordering because there is a very small entropy change associated with it. The increase in the dc susceptibility and the peak in χ_{ac} at 14.5 K occurs close to the antiferromagnetic transition temperature of 14.2 K in $FeBr_2$. This indicates an increase in ordering. It is of short range because there is no contribution to the specific heat as in $FeBr_2$. There is also no magnetoamorphic properties with a field-dependent transition temperature as there is in $FeBr_2$.

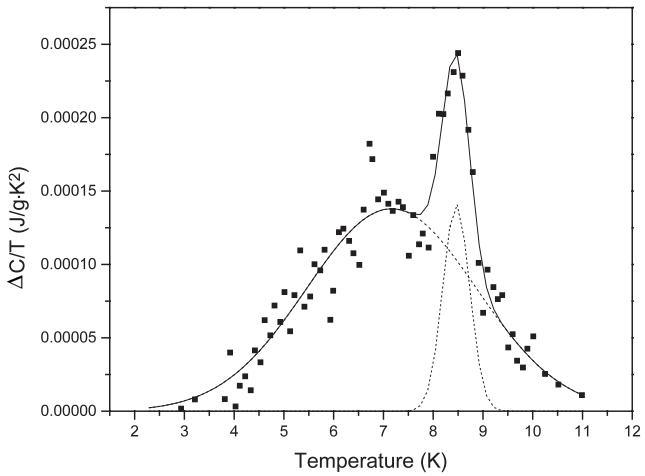

Figure 13. The difference between the zero-field and high field specific heat divided by temperature versus temperature between 3 and 11 K.

Table 1. The $FeBr_2$ GIC parameters of equation (1) for the resistivity ρ_a measured in the (001) plane and ρ_c measured parallel to the c axis.

	ρ_o (Ω cm)	A (Ω cm K)	B (Ω cm K^{-2})
ρ_a	8.7×10^{-4}	1.1×10^{-6}	1.0×10^{-9}
ρ_c	2.7×10^{-2}	4.2×10^{-5}	3.8×10^{-8}

The temperature dependence of the resistivity of most low-stage intercalation compounds is described by

$$\rho = \rho_o + AT + BT^2. \tag{1}$$

The parameters for the best fit of (1) to ρ_a and ρ_c in figure 8 are presented in table 1. Equation (1) describes contributions to the carrier scattering by both in-plane and out-of-plane phonons. The resistivity ρ_o is 32 times larger for ρ_c than for ρ_a because the conductivity is predominantly in the (001) plane. The parameters A and B are both 38 times larger. Thus, after taking into account the change of resistivity, the temperature dependences of ρ_a and ρ_c are the same and that electron–phonon scattering is the dominant scattering process in both directions. The electron hopping mechanism that is suggested to explain ρ_c in some intercalated compounds is not applicable. Therefore, the ratio of the resistance ρ_c/ρ_a is caused by the shape of the Fermi surface. The angular dependence of the magnetoresistance in figure 9 was measured to search for the angular dependent magnetoresistance which was first observed in a quasi-two-dimensional organic conductor [17]. It was observed in the stage-1 and stage-2 $CuCl_2$ GICs [18]. It occurs with a corrugated or undulating Fermi surface in a two-dimensional conductor. The angular dependence in magnetic fields between 3 and 9 T does not show this effect and follows a $\cos^2$ dependence which is expected with a normal metal. There is a chance that it might appear in higher fields that are not available in our laboratory. The angular dependence of the magnetoresistance that was observed indicates that the GIC two-dimensionality of the $FeBr_2$ GIC is not large enough for the angular dependent magnetoresistance effect. This is supported by the fact that the resistance ratio ρ_c/ρ_a is only 30 in the $FeBr_2$ GIC. The relatively small ratio of 30 indicates that there is an undulating Fermi surface to give a component of electron velocity along the c axis.

It is also noteworthy in the resistivity that there is no evidence of the magnetic changes that are indicated in the magnetization. This indicates that there is no appreciable magnetic scattering.

Since the Hall coefficient of the stage-2 $FeBr_2$ GIC is temperature independent between 4.2 and 300 K, the one-carrier model with $R_H = 1/ne$ is used to calculate n, the number of carriers per unit volume. The measured value of $R_H = (4.5 \pm 0.05) \times 10^{-8}$ m^3 C^{-1} gives $n = 1.4 \times 10^{26}$ m^{-3}. This is about one-sixth of those of most stage 2 and 3 GICs [19].

5. Conclusions

$FeBr_2$ can be intercalated into HOPG. A stage-2 sample is made by maintaining $FeBr_2$ powder and graphite at 500 °C for 40 weeks. The c-axis periodicity I_c is 13.14 Å. The dc susceptibility is explained by the Curie–Weiss paramagnetism modified by a temperature-independent van Vleck term in the temperature range 40–300 K. There is magnetic ordering below 14.5 K. Short-range order commences at 14.5 K and long-range ordering indicated by a peak in the specific heat occurs at 8.5 K. There is a spin glass phase below 3.2 K with a long magnetic relaxation time. The amplitude and temperature of the maximum in the dispersion of the ac susceptibility associated with the transition to the spin glass phase is frequency dependent and is fitted to the Vogel–Fulcher law. The ac susceptibility also indicates the magnetic changes at 14.5 and 8.5 K. The transitions at 14.5 and 8.5 K cannot be explained by two-dimensional and three-dimensional ordering, respectively. If the ordering at 8.5 K were long range and three-dimensional, one would expect to see a much larger peak in the specific heat, with an associated entropy nearing that of the theoretical value. The specific heat data for this sample yields only a small fraction of this value. Furthermore, any three-dimensional ordering should be antiferromagnetic, as in pristine $FeBr_2$. In this case, one would expect a decrease in the magnetization as the temperature is lowered through 8.5 K. The data clearly show an increase, implying that this is a ferromagnetic ordering. We believe that the ordering at 14.5 K is short-ranged two-dimensional ordering and that at 8.5 K is of longer range, but still two-dimensional. The electrical resistivity along the c axis and in the (001) plane is explained by the equation that includes both in-plane and out-of-plane scattering. The Hall coefficient is independent of temperature between 4.2 and 300 K and corresponds to a carrier density of 1.4×10^{26} m^{-3}.

Acknowledgments

The research was supported financially by the Natural Sciences and Engineering Research Council of Canada. The highly oriented pyrolytic graphite was provided by Dr A W Moore. Sabbatical leave from Shiraz University to MB is gratefully acknowledged.

References

[1] Katsumata K, Aruga Katori H, Shapiro S M and Shirane G 1997 *Phys. Rev.* B **55** 11466
[2] Aruga Katori H, Katsumata K and Katori M 1996 *Phys. Rev.* B **54** 9620
[3] Fert A R, Carrara P, Lanusse M C, Mischler G and Redoules J P 1973 *J. Phys. Chem. Solids* **34** 223
[4] Pilloth J, Brand R A, Takele S, Pereira de Azevedo M M, Kleemann W, Binck Ch and Kushauer J 1995 *Phys. Rev.* B **52** 15372
[5] Suzuki M and Suzuki I S 1998 *Phys. Rev.* B **58** 371
[6] Balestri C, Vangeliste R, Melin J and Herold A 1974 *C. R. Acad. Sci., Paris* **279** 279
[7] Stahl H 1977 *Z. Anorg. Alloy Chem.* **428** 269
[8] Stumpf E 1977 *Mater. Sci. Eng.* **31** 53
[9] Stumpf E, Schubert P and Ehrhardt C 1989 *Synth. Met.* **34** 73

[10] Montgomery H C 1971 *J. Appl. Phys.* **42** 2971
[11] Jacobs I S and Lawrence P E 1964 *J. Appl. Phys.* **35** 996
[12] Silverstwin S D and Jacobs I S 1964 *Phys. Rev. Lett.* **12** 670
[13] Jacobs I S and Lawrence P E 1967 *Phys. Rev.* **164** 866
[14] Oguro I, Suzuki M and Yasuoka H 1985 *Synth. Met.* **12** 449
[15] El Hafidi M, Chouteau G and Yazami R 1989 *Synth. Met.* **34** 525
[16] Mydosh J A 1993 *Spin Glasses: An Experimental Introduction* (Washington, DC: Taylor and Francis)
[17] Kajita K, Nishio Y, Takahashi T, Sasaki W, Kato R, Kobayashi H, Kobayashi A and Iye Y 1989 *Solid State Commun.* **70** 1189
[18] Sato H, Andersson O E, Enoki T, Suzuki I S and Suzuki M 2000 *J. Phys. Soc. Japan* **69** 1136
[19] Barati M, Dube P A, Ummat P K and Datars W R 1998 *Solid State Commun.* **107** 35